

# Origin, evolution, and fate of Titan's polar clouds

Received: 24 August 2025

Accepted: 19 November 2025

Published online: 04 December 2025

 Check for updatesBruno de Batz de Trenquelléon <sup>1,2,3</sup>✉, Pascal Rannou <sup>1</sup>,  
Sébastien Lebonnois <sup>2</sup> & Sandrine Vinatier<sup>3</sup>

Saturn's moon Titan exhibits a rich interplay of atmospheric chemistry and meteorology, including the seasonal formation of polar stratospheric clouds, first observed by Voyager and later by the Cassini mission. Using a global climate model with haze and cloud microphysics, we investigate their origin, evolution, and fate. We find that cloud formation begins in early autumn, triggered by rapid radiative cooling and chemical enrichment within the stratospheric polar vortex. Initially extending to 336 km altitude and composed of benzene and hydrogen cyanide ices, these clouds descend to lower altitudes during autumn and winter, evolving in composition as additional species condense, before dissipating in spring. This process reflects a unified, hemisphere-spanning seasonal mechanism shaping Titan's climate. Our model explains observed seasonal patterns and predicts the onset of the next northern polar cloud in 2027. These results provide a predictive framework for future Titan observations, missions, and long-term climate evolution studies.

Polar clouds were long detected in the northern polar region shortly after the spring equinox, using the InfraRed Interferometer Spectrometer onboard Voyager (November 1980;  $L_S = 9.1^\circ$ ). Clouds were first inferred from the opacity they generate in the low stratosphere<sup>1,2</sup> and, in a more specific way, with spectroscopic signatures of condensate species such as  $C_4N_2$ ,  $HC_3N$ , and  $C_2H_2$ <sup>3,4</sup>. Later, tropospheric polar clouds were directly imaged in the southern polar region during spring and summer, using large ground-based telescopes<sup>5–7</sup> (from October 1998 to January 2005;  $L_S = 216.8^\circ$ – $300.6^\circ$ ). These scattered events constituted the first hints, still indecipherable, of a polar cloud cycle.

At the very beginning of the Cassini mission in the Saturnian system, both the Imaging Science Subsystem (ISS) and the Visual and Infrared Mapping Spectrometer (VIMS) monitored convective tropospheric clouds in the southern polar regions<sup>8</sup> (from April to December 2004;  $L_S = 290.3^\circ$ – $299.3^\circ$ ). The same year, VIMS carried out its first observations of Titan's northern hemisphere. In December 2004, it revealed the edge of a first polar cloud structure<sup>9</sup>. This cloud, initially observed between latitude  $51^\circ N$  and the terminator at  $68^\circ N$ , was estimated to lie between 30 and 65 km in altitude, in the region where  $CH_4$

and  $C_2H_6$  can condense<sup>10</sup>. In December 2006 ( $L_S = 326.7^\circ$ ), while the north polar region gradually emerged from the polar night, it brought to light a much more complex and widespread cloud structure, covering the entire polar region<sup>11,12</sup>. Spectral analyses from the Composite Infrared Spectrometer (CIRS) and VIMS revealed the presence of HCN ice and  $HC_3N$  ice within this cloud, with cloud top reaching 165 km at  $70^\circ N$  and 150 km at  $62^\circ N$ <sup>13,14</sup>. This structure began to dissipate gradually in March 2009 ( $L_S = 355.7^\circ$ ) as Titan approached equinox, and was observed until June 2010 ( $L_S = 10.5^\circ$ ), when only residual traces remained above the north pole<sup>12,14,15</sup>. A season later, shortly after the southern autumnal equinox, a large stratospheric cloud structure was identified above the south pole by ISS<sup>16,17</sup>, beginning in April 2012 ( $L_S = 32.1^\circ$ ). This detection was later confirmed by VIMS<sup>18</sup> and CIRS<sup>19</sup>. Images acquired in May 2012 ( $L_S = 33.7^\circ$ ) show a cloud centered above the south pole, at latitudes higher than  $80^\circ S$ , and measured at an altitude of  $300 \pm 10$  km<sup>17</sup>, with a top at  $322 \pm 25$  km<sup>16</sup>. It remains unclear whether the cloud formed in April 2012<sup>16</sup> or, as suggested by limb images taken in September 2011<sup>17</sup> ( $L_S = 25.8^\circ$ ), whether its formation began earlier, following a sharp decrease in stratospheric temperature,

<sup>1</sup>Groupe de Spectrométrie Moléculaire et Atmosphérique (GSMA), Université de Reims Champagne-Ardenne, CNRS, Reims, France. <sup>2</sup>Laboratoire de Météorologie Dynamique (LMD/IPSL), Sorbonne Université, ENS, PSL Research University, Ecole Polytechnique, Institut Polytechnique de Paris, CNRS, Paris, France. <sup>3</sup>LIRA, Observatoire de Paris, Université PSL, Sorbonne Université, Université Paris Cité, CY Cergy Paris Université, CNRS, Meudon, France.

✉ e-mail: [bruno.debatz@obspm.fr](mailto:bruno.debatz@obspm.fr)

along with a significant increase in molecular gas concentrations detected by CIRS<sup>18,20,21</sup> over Titan's south polar region between May 2011 ( $L_S = 21.7^\circ$ ) and February 2012 ( $L_S = 30.8^\circ$ ). Until the end of the Cassini mission in 2017, the cloud evolved in both horizontal extent and vertical thickness<sup>14,16</sup>. In April 2013 ( $L_S = 44.2^\circ$ ), it reached  $75^\circ\text{S}$  latitude and expanded to  $58^\circ\text{S}$  by April 2017 ( $L_S = 89.7^\circ$ ), while its top decreased in altitude compared to 2012. Spectral analysis revealed the presence of condensed HCN from 2012<sup>18</sup>, followed by the first detection of  $\text{C}_6\text{H}_6$  ice in 2013<sup>22</sup>.

Despite an abundance of high-quality observations, the formation of the northern polar cloud and the final stages of the southern polar cloud during winter could not be observed due to the timing of the Cassini mission. As a result, the formation mechanisms of these clouds and their complete seasonal cycle are not yet fully understood. For instance, it is not clearly established if the south and the north clouds are two ends of the polar system, and if the cloud cycle is symmetric between the two polar regions. Furthermore, the composition and size of the cloud particles, the fate of the chemical species once condensed and their role in surface-atmosphere interactions are not yet determined.

We explore the mechanisms governing the formation and evolution of Titan's polar clouds using the Titan Planetary Climate Model<sup>23,24</sup> (Titan PCM), coupled with a microphysical haze and cloud model ("Methods"). The Titan PCM predicts three main condensation layers<sup>24</sup>. The first, located between 5 and 25 km altitude, consists of « massive

tropospheric clouds » primarily composed of methane. These clouds develop within the ascending branches of the atmospheric circulation, at mid-latitudes in the spring and summer hemisphere. The second layer, situated near the tropopause between 30 and 75 km altitude, corresponds to a cold region oversaturated with trace hydrocarbons (e.g.,  $\text{C}_2\text{H}_6$ ) and nitriles (e.g., HCN) that persist throughout the year. This region of condensed hydrocarbons and nitriles is present across the entire planet, with greater density in the polar regions during spring and summer (Fig. 1 and Supplementary Fig. 1). In the following sections, we will refer to this layer as the « condensed mist ». Finally, the third condensation layer, which is the main focus of this study, lies at high-altitude, between 75 and 350 km. We will refer to these high-altitude structures, typical of Titan's polar regions, as « polar clouds ». The fundamental differences between these three condensation regions lie in their respective lifetimes and cloud particle sizes: a few Titan days for the massive tropospheric clouds, roughly half a Titan year for the polar clouds, and a continuous presence throughout the year for the condensed mist. The corresponding droplet sizes are larger than 100, 10, and  $1\ \mu\text{m}$ , respectively.

The Titan PCM predicts a similar evolution of the northern and southern polar clouds, with quantitative differences which can be related to Titan's orbital eccentricity (Fig. 1 and Supplementary Fig. 1). Since more observations are available for the southern polar cloud, particularly regarding its genesis and early stages of evolution, we focus primarily on the evolution of this cloud. We find that the timeline

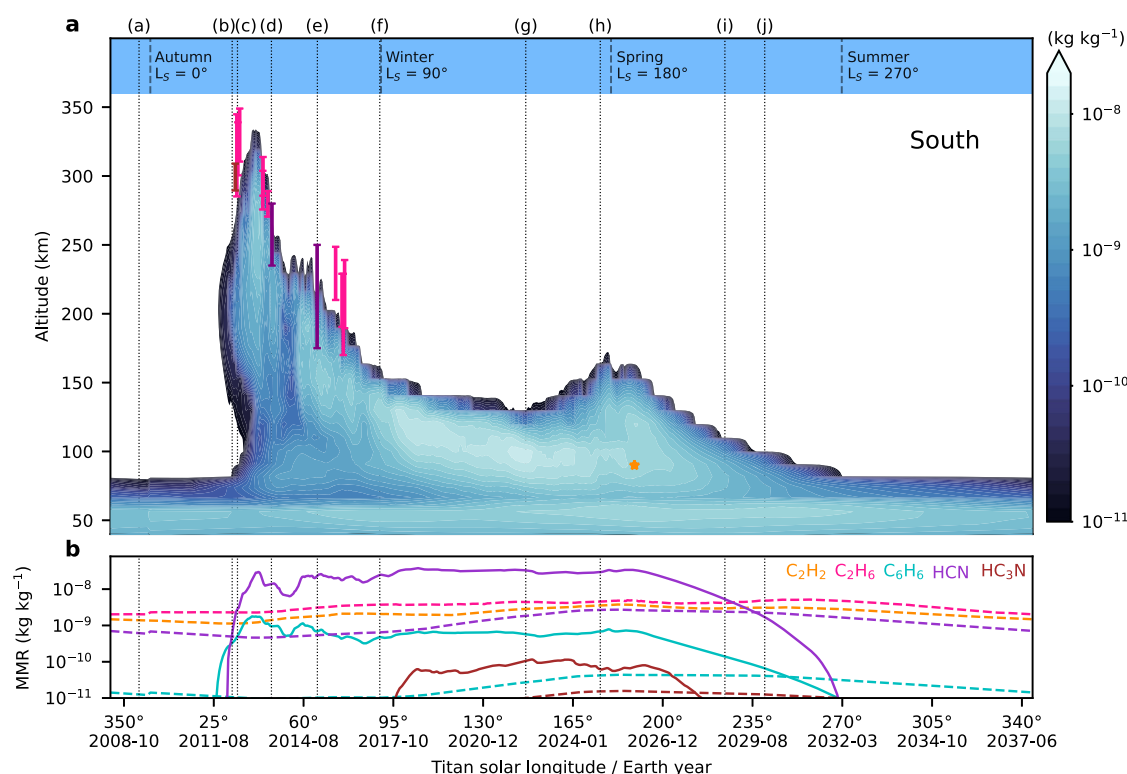


**Fig. 1 | Modeling the annual evolution of Titan's southern polar cloud.**

**a** Simulated evolution of the zonally averaged total ice mass mixing ratio, over poleward latitudes higher than  $60^\circ\text{S}$ . Altitudes estimated from the Imaging Science Subsystem (ISS) observations are shown in brown<sup>17</sup> and pink<sup>16</sup>, and those from the Composite Infrared Spectrometer (CIRS) observations are shown in purple<sup>22</sup>. The altitude estimated from Voyager measurements is indicated with an orange star<sup>3</sup>. The polar cloud evolves between altitudes of 75 and 336 km. Below 75 km, the region remains supersaturated in minor species throughout the year. **b** Simulated evolution of the zonally averaged mass mixing ratio of each ice above 75 km (color solid curves) and between 30 and 75 km (color dashed curves). Vertical lines correspond to key phases of the polar cloud evolution, depending on Titan's season and solar longitude ( $L_S$ ): **a** March 2009 ( $L_S = 355.7^\circ$ ), end of southern summer,

before cloud formation; **b** April 2012 ( $L_S = 32.1^\circ$ ), first detection of the southern polar cloud<sup>16</sup>; **c** June 2012 ( $L_S = 34.5^\circ$ ), observation of the cloud patch near Titan's south pole<sup>17</sup>; **d** July 2013 ( $L_S = 47.7^\circ$ ) and **e** February 2015 ( $L_S = 65.3^\circ$ ), detection of  $\text{C}_6\text{H}_6$  ice in the southern polar cloud<sup>22</sup>; **f** April 2017 ( $L_S = 89.7^\circ$ ), end of southern autumn, last observation of the southern polar cloud<sup>14</sup>; **g** May 2022 ( $L_S = 146.5^\circ$ ), mid-southern winter, corresponding season of the northern polar cloud observation in December 2006<sup>22</sup>; **h** December 2024 ( $L_S = 175.7^\circ$ ), corresponding season of the northern late-winter annular opacity feature observation<sup>12</sup>; **i** October 2028 ( $L_S = 224.2^\circ$ ), beginning of southern spring, analogous season of northern polar cloud dissipation<sup>14</sup>; **j** January 2030 ( $L_S = 239.9^\circ$ ), disappearance of the polar cloud in the model during the second half of spring.

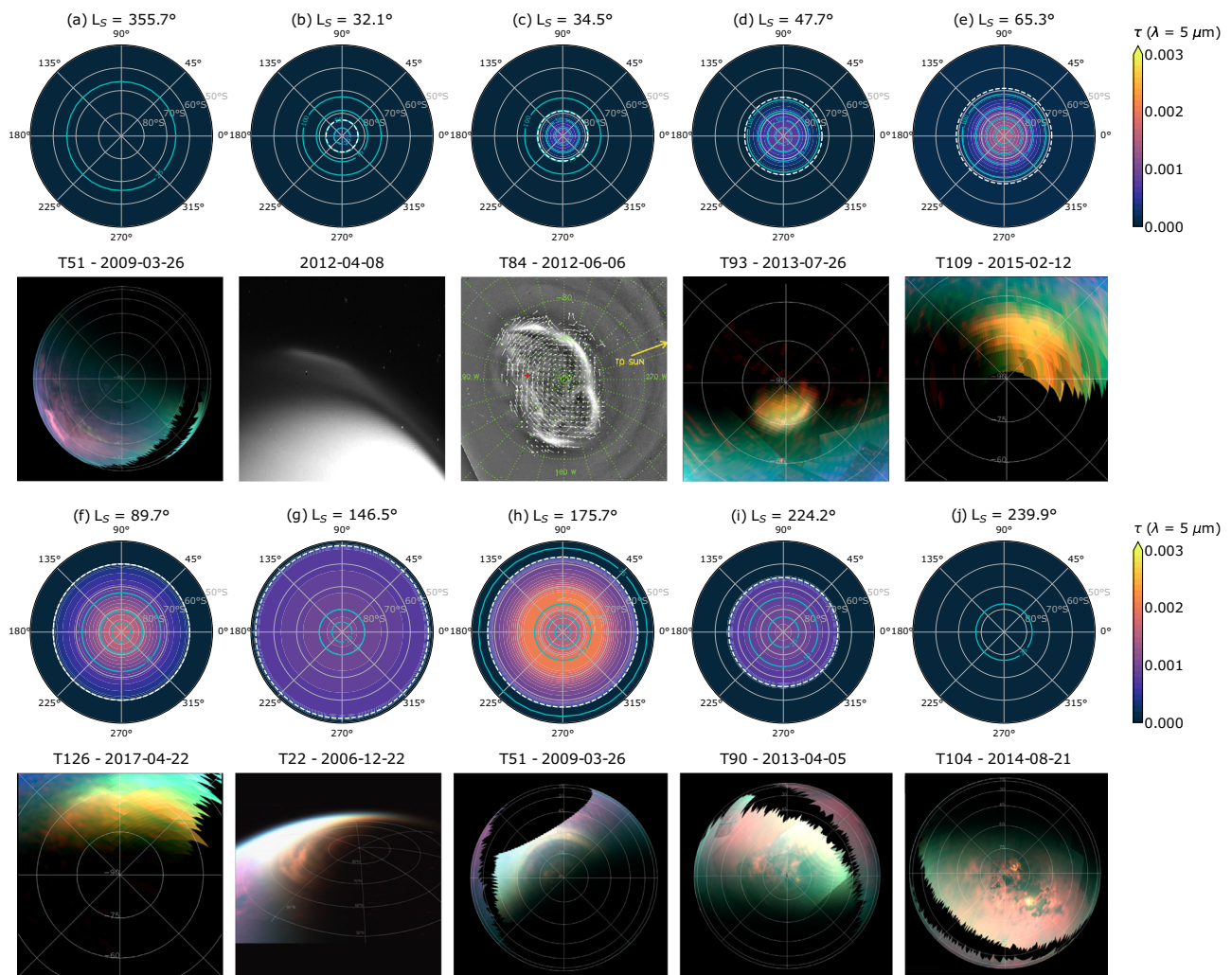


**Fig. 2 | Latitudinal evolution of the polar clouds.** Polar maps of modeled cloud opacity  $\tau$  at wavelength  $\lambda = 5 \mu\text{m}$  and an altitude above 75 km (first and third rows) compared to observations from Cassini's flybys T of Titan<sup>12,14,16,17</sup> (second and fourth rows). The coordinates grid on the modeled maps show latitudes every  $10^\circ$  and longitudes every  $45^\circ$ . The white dashed circles represent the maximum horizontal extent of the cloud. The blue contours indicate the zonal wind speed within the

polar cloud region, between altitudes of 75 km and 350 km. Observations (a–f) (respectively (g–j)) refer to the south pole (respectively the north pole) and correspond to the seasons associated with the solar longitude ( $L_S$ ) key phases shown in Fig. 1. Additional information regarding these observations is provided in Supplementary Table 1.

of the southern polar cloud in the Titan PCM, and compared at each step ((a) through (j)) with observations, can be described as follows.

## Results

### Formation processes of polar clouds on Titan

Before the southern autumnal equinox in August 2009 ( $L_S = 0.0^\circ$ ), no polar cloud is present above the south pole (Fig. 1a). This is confirmed by observations from the T51 flyby (March 26, 2009;  $L_S = 355.7^\circ$ ), which show a clear sky over the south pole (Fig. 2a).

At the beginning of autumn, the model predicts that the descent of polar air from the atmospheric circulation cell brings down to the core of the newly formed polar vortex the chemical species produced several hundred kilometers higher (Supplementary Fig. 2), along with Titan's photochemical aerosols. This process is illustrated in the model by a marked increase in poleward horizontal fluxes of chemical species starting in August 2011 (Supplementary Fig. 3;  $L_S = 25.3^\circ$ ), and has been characterised by CIRS<sup>18,20,21</sup> (Supplementary Fig. 4). The thermal infrared emission to space of these atmospheric compounds, combined with the beginning of the polar night at the south pole, leads to significant cooling in the stratosphere. Between March 2009 ( $L_S = 355.7^\circ$ ) and October 2011 ( $L_S = 27.3^\circ$ ), the stratosphere cooled by 30.3 K above

the south pole at an altitude of 200 km (Supplementary Fig. 5). The combination of this chemical enrichment (Supplementary Figs. 2–4) and cooling (Supplementary Fig. 5) triggers the nucleation of  $\text{C}_6\text{H}_6$  on aerosols in October 2011, followed by its condensation (Fig. 1b). Consequently, the enhancement in scattered sunlight above the south pole observed on September 2011<sup>17</sup> is more likely attributable to a local enrichment of haze caused by the circulation, rather than to condensation marking the initial stages of the southern polar cloud formation, which actually begins later, at the end of 2011.

At the beginning of 2012, the southern stratospheric temperature continued to decrease (Supplementary Fig. 5), promoting further cloud development and condensation at higher altitudes. Once the nucleation threshold of  $\text{C}_6\text{H}_6$  is reached in October 2011, the condensation of HCN on cloud condensation nuclei becomes easier ("Methods"), beginning a few months later, in March 2012 ( $L_S = 31.5^\circ$ ). The model therefore predicts that HCN can condense in Titan's stratosphere with temperatures near 130 K, consistent with previous estimates<sup>18</sup>, and that cloud properties can be reproduced under these conditions, approximately 30 K warmer than predicted by earlier models<sup>25</sup>. The onset of HCN condensation, which produces an ice mixing ratio ten times higher than that of  $\text{C}_6\text{H}_6$  (Supplementary Fig. 6),

coincides with the first observations of the southern polar cloud in April 2012<sup>16</sup> ( $L_S = 32.1^\circ$ ).

These modeled condensed species are confined within the polar vortex (Fig. 2 and Supplementary Fig. 2), trapped by a strong jet stream that creates a barrier, preventing mixing between polar and mid-latitude air masses. This mechanism thus limits the latitudinal extent of the southern polar cloud to poleward regions (Fig. 2b). Observational evidences of zonal winds and molecular abundances<sup>26</sup> confirmed that the stratospheric cloud cannot extend into or beyond the polar vortex, where molecular abundances are significantly lower and temperatures higher, inhibiting mid-latitudes cloud formation.

Few months later, in mid-2012, the cloud reaches titanic proportions in the model. It now extends from 130 to 336 km in altitude (Fig. 1), with a thickness exceeding 200 km above the pole and a peak condensation near 300 km, similar to the cloud altitudes observed between May 2012 ( $L_S = 33.7^\circ$ ) and April 2013 ( $L_S = 44.0^\circ$ ) by ISS<sup>16,17</sup> and VIMS<sup>18</sup>. The cloud remains confined within the polar vortex, covering the south pole up to  $79^\circ\text{S}$  latitude (Fig. 2c and Supplementary Fig. 2), as observed during the T84 flyby (June 06, 2012;  $L_S = 34.5^\circ$ ). The modeled cloud is structured in distinct layers: a layer of pure  $\text{C}_6\text{H}_6$  ice between 315 and 336 km, a mixture of  $\text{C}_6\text{H}_6$  and HCN ices between 150 and 315 km, and finally a layer of dominantly HCN ice between 130 and 150 km (Supplementary Fig. 6).

### Seasonal variations of Titan's polar clouds

As autumn progresses, the temperature in the polar upper stratosphere ( $>200$  km) increases over time (Supplementary Fig. 5) due to enhanced subsidence, which strengthens the adiabatic warming in this region<sup>23</sup>. While the top of the cloud continues to be supplied with chemical species, they now condense at lower altitudes, following locations where temperatures remain cold enough, thereby reducing the vertical extent of the cloud (Fig. 1). Between 2013 and 2017, the top of the cloud descends from 275 km in July 2013 ( $L_S = 47.7^\circ$ ) to 225 km in February 2015 ( $L_S = 65.3^\circ$ ), and down to 160 km in April 2017 ( $L_S = 89.7^\circ$ ), with a vertical extent of 80 km (Fig. 1d–f), in good agreement with the recent observations<sup>16</sup>.

Below 200 km altitude, the weaker zonal winds reduce the intensity of the polar vortex, resulting in a less pronounced confinement of chemical species enrichment toward the pole<sup>23,27,28</sup> (Supplementary Fig. 2). This allows the cloud to extend in latitude, reaching  $75^\circ\text{S}$  in July 2013,  $68^\circ\text{S}$  in February 2015, and  $59^\circ\text{S}$  in April 2017 (Fig. 2d–f), in agreement with the observations<sup>14</sup>. This mechanism may explain why the polar cloud is observed at lower altitudes farther from the pole<sup>14,16,22</sup>.

The Titan PCM predicts that  $\text{C}_6\text{H}_6$  primarily condenses between 160 and 275 km in July 2013, between 120 and 225 km in February 2015, and between 100 and 160 km in April 2017 (Supplementary Fig. 6). This is consistent with the detections of  $\text{C}_6\text{H}_6$  ice at 280 km in July 2013 and between 170 and 250 km in February 2015<sup>22</sup>. HCN condenses at lower altitudes: mainly between 150 and 260 km in July 2013, 110 and 205 km in February 2015, and 75 to 145 km in April 2017 (Supplementary Fig. 6). The evolution of the cloud toward lower and colder altitudes enables other species to condense in the model (Fig. 1). From December 2016 onwards ( $L_S = 85.5^\circ$ ),  $\text{HC}_3\text{N}$  begins to condense between 90 and 130 km (Supplementary Fig. 6), indicating that by late autumn, the cloud is composed of a variety of ices formed from chemical species present in Titan's atmosphere.

During most of the winter period (southern hemisphere: 2017–2022,  $L_S = 90.0$ – $146.5^\circ$ ; northern hemisphere: 2002–2006,  $L_S = 270.0$ – $326.7^\circ$ ), the cloud is in a steady state and undergoes very little change. The cloud top remains at a maximum altitude of about 145 km (Fig. 1g), continuously supplied with chemical species by the descending air from the global circulation, which persists throughout autumn and winter. However, it can be observed that in winter, the polar vortex weakens in the model (Fig. 2g and Supplementary Fig. 2),

leading to a faster horizontal expansion of the cloud, which reaches latitudes down to about  $55^\circ\text{S}$  in May 2022 ( $L_S = 146.5^\circ$ ).

At lower altitudes ( $<75$  km), the condensed mist condensation intensifies (Fig. 1g), which is consistent with the observation of northern winter  $\text{C}_2\text{H}_6$  clouds between 35 and 60 km in December 2004<sup>9</sup> ( $L_S = 299.3^\circ$ ).

### Final phase and dissipation of Titan's polar clouds

At the end of winter (southern hemisphere: 2022–2025,  $L_S = 146.5$ – $180.0^\circ$ ; northern hemisphere: 2006–2009,  $L_S = 326.7$ – $0.0^\circ$ ), subsidence weakens in the model (Supplementary Figs. 2 and 3). Adiabatic heating decreases, giving way to dominant radiative cooling. As a result, the temperature in the cloud region decreases slightly (Supplementary Fig. 7). Simultaneously, a small secondary meridional wind cell emerges in the winter hemisphere ( $>70^\circ$ ), opposite to the main meridional circulation cell, at altitudes between 100 and 400 km (Supplementary Fig. 2). This cell, associated with the overall destabilization of the main cell, is unstable, forming and dissipating rapidly within the cloud region, and preferentially enriches the high latitudes ( $\sim 75^\circ$ ) in molecules rather than the pole. The cooling, combined with this circulation cell, enables the cloud to redevelop at latitudes near  $75^\circ\text{S}$ , extending vertically between 75 and 160 km (Fig. 1h). The situation is symmetrical between the southern and northern winter hemispheres. Therefore, the late winter ring-shaped structure observed in the north by Cassini during the T51 flyby (March 26, 2009;  $L_S = 355.7^\circ$ ), linked to the cloud dissipation of its inner part and to the depletion of aerosols at the pole through wet deposition<sup>14,26</sup>, would also be reinforced by the recent development of the cloud at high latitudes (Fig. 2h).

The model now provides an explanation for the observation of a stable winter cloud layer in the northern polar region, located around  $100 \pm 20$  km altitude, above the condensed mist, as detected by VIMS between December 2006 and May 2009<sup>26</sup> ( $L_S = 326.7$ – $357.1^\circ$ ). Furthermore, according to the model, the  $\text{C}_6\text{H}_6$  and  $\text{HC}_3\text{N}$  condense mainly poleward ( $>70^\circ$ ), while HCN extends to lower latitudes (beyond  $55^\circ$ ). As a result, the cloud is more opaque above the pole than at mid-latitudes. This was observed at the north pole at the end of winter in May 2009 ( $L_S = 357.1^\circ$ ), where the clouds extended from  $64^\circ\text{N}$  up to the north pole and were surrounded by a diffuse hood reaching down to  $55^\circ\text{N}$ <sup>12</sup>.

After the southern spring equinox in April 2025 ( $L_S = 180.0^\circ$ ), the south pole emerges from the polar night, leading to a warming of the region. Moreover, due to the reversal of atmospheric circulation, the pole is no longer supplied with chemical species in the Titan PCM<sup>23</sup> (Supplementary Figs. 2 and 3), as observed by CIRS<sup>27</sup>. The cloud therefore begins to dissipate (Fig. 1i). This event in the south polar region mirrors the gradual dissipation observed for the northern polar cloud after the northern spring equinox in August 2009<sup>14</sup> ( $L_S = 0.0^\circ$ ). Polar clouds therefore, remain for some time after the spring equinox. This persistence was confirmed by Voyager's observations of the north pole a few months after the northern spring equinox, in November 1980 ( $L_S = 9.1^\circ$ ), which still revealed condensate signatures in this region<sup>3,4</sup>.

Eventually, the polar cloud completely disappears in the model four years after the equinox (Fig. 2j). This conclusion is supported in particular by the T104 flyby in August 2014 ( $L_S = 59.9^\circ$ ), which revealed the appearance of small convective clouds and surface features such as lakes and seas in the northern hemisphere<sup>14</sup>, as well as by ground-based southern hemisphere observations from mid-spring onward in 1988 that detected tropospheric convective clouds<sup>5–7</sup>.

## Discussion

Our results show that the polar clouds observed in the northern hemisphere in 2006 and in the southern hemisphere from 2012 are the two ends of the polar cloud's life. Based on this, we can predict that a new polar cloud should form in the northern polar stratosphere around the end of 2027. This cloud should be large enough to be detected from Earth at altitudes above 300 km during 2028, thanks to

spectroscopic observations from the James Webb Space Telescope. For instance, the NIRSpc instrument should enable the identification of HCN ice, while MIRI's extended spectral coverage would facilitate the investigation of additional ice species. However, MIRI's broad field of view would complicate the isolation of spectral features specific to the polar stratospheric cloud. By around 2030, it may also be visually confirmed and spectrally detected with first observations from the Extremely Large Telescope in spectral ranges minimizing the terrestrial atmospheric impact.

Formed at very high altitudes and composed of small particles ( $1\ \mu\text{m} < r_{\text{clouds}} < 40\ \mu\text{m}$ , Supplementary Fig. 8), the polar clouds exhibit relatively slow precipitation rates and tend to re-evaporate before reaching the surface (Supplementary Fig. 6). This process releases much of their compounds back into the lower stratosphere in gaseous form, where both the vapor abundance and the saturation ratio of minor species are lower than those in the upper stratosphere (Supplementary Fig. 4). Only about 10% of the ices produced above 100 km precipitates down to the surface (Supplementary Fig. 9). Since polar clouds develop at lower altitudes toward their margins, the precipitation of their constituent ices is favored at mid-latitudes, peaking around  $50^\circ$ , mainly during spring and summer, following cloud dissipation. Radio occultation measurements have revealed a cold region above the pole throughout the winter, between 75 and 150 km altitude<sup>29</sup>. This feature is not yet accurately reproduced by models, where it remains confined to 75–120 km in the Titan PCM (Supplementary Fig. 5). If the model were able to more accurately reproduce this cold region, the polar cloud would likely extend to higher altitudes, as suggested by CIRS observations at the end of the northern winter (Supplementary Fig. 1). Nevertheless, the impact on precipitation rates would remain negligible, given the low sedimentation velocities of cloud particles and the higher altitude of condensation.

In contrast,  $\text{CH}_4$  and  $\text{C}_2$  ices form below 75 km, facilitating their deposition onto the surface (Supplementary Fig. 9). Titan's topography shapes near-surface atmospheric dynamics, creating an asymmetric distribution of its precipitation, and even prevents  $\text{C}_2\text{H}_6$  precipitation in the northern hemisphere. At low latitudes, their precipitation trend mirror that of  $\text{CH}_4$ , suggesting co-precipitation during  $\text{CH}_4$  rainfall events at the equator during the equinoctial season<sup>30</sup>. The intense  $\text{CH}_4$  precipitation rate over the north pole arises from local lakes, where evaporated  $\text{CH}_4$  during summer rapidly saturates the atmosphere and precipitates into the same region. Over hundreds of millions of years, this could lead to the accumulation on Titan's surface of several tens of millimeters of  $\text{C}_6\text{H}_6$  and  $\text{HC}_3\text{N}$ , and several tens of meters of  $\text{C}_2\text{H}_2$  and  $\text{C}_2\text{H}_6$  and HCN, contributing to the composition of Titan's surface and lakes. The precipitation predicted by our model offers insights into the evolving composition of the polar lakes over time, as well as into the surface humidity of equatorial regions on shorter timescales, helping to anticipate future observations by the Dragonfly mission.

## Methods

### Model

The Titan Planetary Climate Model (Titan PCM) is based on previous modeling studies of Titan's atmosphere<sup>23,24</sup>, while incorporating higher resolution and an expanded set of chemical species in the cloud microphysics module. The atmospheric domain is discretized on a 32-longitude  $\times$  64-latitude grid ( $11.25^\circ \times 2.81^\circ$ ) with 55 vertical levels extending from the surface to approximately 500 km altitude. At each grid point, the dynamical core computes the transport of atmospheric constituents (gases, aerosols, and ices) 16,000 times per Titan day, corresponding to a dynamical timestep of 1 min 30 s. The physical parameterizations compute haze and cloud microphysics, boundary-layer turbulent mixing, dry convective adjustment, and subsurface thermal conduction 400 times per Titan day. Radiative transfer is evaluated 40 times per Titan day, while the photochemical solver is executed four times per Titan day.

### Haze processes

The haze microphysics module integrated into the Titan PCM employs a moment-based representation of a bimodal aerosol population, allowing simultaneous treatment of small spherical particles and large fractal aggregates while avoiding the computational cost of bin-resolved schemes<sup>24,31</sup>. The model calculates production, coagulation, and sedimentation for both aerosol modes. Injection of spherical aerosols produced by high-altitude photochemistry is imposed at the model top according to a Gaussian production profile. Intramodal and intermodal Brownian coagulation for both spherical and fractal aerosols is explicitly solved. Sedimentation is treated using a flux-form scheme with a first-order slip-flow correction. Aerosol properties are prescribed as follows:

- Aerosol density:  $\rho = 800\ \text{kg m}^{-3}$ ;
- Production radius of spherical aerosols:  $r_p = 10\ \text{nm}$ ;
- Monomer radius:  $r_m = 50\ \text{nm}$ ;
- Fractal dimension of aerosols:  $D_f = 2.0$ ;
- Electric charge of aerosols:  $n_e = 15\ \mu\text{m}^{-1}$ .

### Cloud processes

The cloud microphysics module is designed to simulate the physical processes of nucleation, condensation/sublimation, and sedimentation<sup>24,32</sup> for six key species involved in Titan's cloud formation:  $\text{CH}_4$ ,  $\text{C}_2\text{H}_2$ ,  $\text{C}_2\text{H}_6$ ,  $\text{C}_6\text{H}_6$ , HCN, and  $\text{HC}_3\text{N}$ . When the nucleation of one species is triggered, all species can condense simultaneously onto aerosols acting as cloud condensation nuclei (CCN). However, the model does not consider the co-condensation of species onto aerosols<sup>33,34</sup>, and they therefore condense independently of each other.

### Photochemistry and radiative transfer

The photochemical solver is based on updated spectroscopic data and includes only neutral chemistry<sup>23</sup>. The reaction scheme is solved independently in each 1D column, extending from the surface to 1300 km altitude, and comprises 43 chemical species participating in 323 reactions.

The radiative transfer scheme employs a correlated-k method with 23 narrow bands in the visible range and 23 in the infrared, spanning wavelengths from 0.3 to 10,000  $\mu\text{m}$ <sup>23</sup>. Absorption by  $\text{CH}_4$ ,  $\text{C}_2\text{H}_6$ ,  $\text{C}_2\text{H}_2$ , and HCN is included. Spectroscopic tables are generated on a 2D grid of 10 pressure bins ( $10^{-1}$ – $10^6$  Pa) and eight temperature bins (60–200 K). Collision-induced absorption is treated as continuum opacity, and Rayleigh scattering is accounted for. Radiative transfer is fully coupled with the chemical and microphysical modules. The radiative transfer equations are solved under the plane-parallel approximation using a two-stream source-function method.

### Initial conditions and simulation setup

The reference simulation presented here includes both haze and cloud microphysics, fully coupled to the radiative transfer module.

The simulation was initialized without any pre-existing clouds and the modeled clouds were allowed to evolve freely over a period of 50 Titan years. The interannual variations in the polar cloud cycle become negligible after 30 years, and we present here the average of the last four years of simulation.

### Data availability

The Titan PCM simulation data generated in this study have been deposited in the IPSL Data Catalog database under accession code <https://doi.org/10.14768/85b9e037-57a2-46b5-945b-23a02e32aca235>.

### Code availability

The Titan PCM code is publicly available online under accession code <https://svn.lmd.jussieu.fr/Planeto/trunk/LMDZ.TITAN/> and is described in detail in previous relevant publications<sup>23,24</sup>.

## References

- Samuelson, R. E. Radiative equilibrium model of Titan's atmosphere. *Icarus* **53**, 364–387 (1983).
- Samuelson, R. E. & Mayo, L. A. Thermal infrared properties of Titan's stratospheric aerosol. *Icarus* **91**, 207–219 (1991).
- Samuelson, R. E., Mayo, L. A., Knuckles, M. A. & Khanna, R. J. C<sub>4</sub>N<sub>2</sub> ice in Titan's north polar stratosphere. *Planet. Space Sci.* **45**, 941–948 (1997).
- Khanna, R. K. Condensed species in Titan's stratosphere: confirmation of crystalline cyanoacetylene (HC<sub>3</sub>N) and evidence for crystalline acetylene (C<sub>2</sub>H<sub>2</sub>) on Titan. *Icarus* **178**, 165–170 (2005).
- Roe, H. G., de Pater, I., Macintosh, B. A. & McKay, C. P. Titan's clouds from gemini and keck adaptive optics imaging. *Astrophys. J.* **581**, 1399–1406 (2002).
- Hirtzig, M. et al. Monitoring atmospheric phenomena on Titan. *Astron. Astrophys.* **456**, 761–774 (2006).
- Porco, C. C. et al. Imaging of Titan from the Cassini spacecraft. *Nature* **434**, 159–168 (2005).
- Brown, R. H. et al. Observations in the Saturn system during approach and orbital insertion, with Cassini's visual and infrared mapping spectrometer (VIMS). *Astron. Astrophys.* **446**, 707–716 (2006).
- Griffith, C. A. et al. Evidence for a polar ethane cloud on Titan. *Science* **313**, 1620–1622 (2006).
- Rannou, P., Montmessin, F., Hourdin, F. & Lebonnois, S. The latitudinal distribution of clouds on Titan. *Science* **311**, 201–205 (2006).
- Rodriguez, S. et al. Global circulation as the main source of cloud activity on Titan. *Nature* **459**, 678–682 (2009).
- Le Mouélic, S. et al. Dissipation of Titan's north polar cloud at northern spring equinox. *Planet. Space Sci.* **60**, 86–92 (2012).
- Anderson, C. M., Samuelson, R. E., Bjoraker, G. L. & Achterberg, R. K. Particle size and abundance of HC<sub>3</sub>N ice in Titan's lower stratosphere at high northern latitudes. *Icarus* **207**, 914–922 (2010).
- Le Mouélic, S. et al. Mapping polar atmospheric features on Titan with VIMS: from the dissipation of the northern cloud to the onset of a southern polar vortex. *Icarus* **311**, 371–383 (2018).
- Brown, M. E., Roberts, J. E. & Schaller, E. L. Clouds on Titan during the Cassini prime mission: a complete analysis of the VIMS data. *Icarus* **205**, 571–580 (2010).
- Hanson, L. E., French, R., Waugh, D. W., Barth, E. L. & Anderson, C. M. The evolution of Titan's cold south polar cloud. *Geophys. Res. Lett.* **52**, e2024GL113415 (2025).
- West, R. A. et al. Cassini imaging science subsystem observations of Titan's south polar cloud. *Icarus* **270**, 399–408 (2016).
- de Kok, R. J., Teanby, N. A., Maltagliati, L., Irwin, P. G. J. & Vinatier, S. HCN ice in Titan's high-altitude southern polar cloud. *Nature* **514**, 65–67 (2014).
- Jennings, D. E. et al. First observation in the South of Titan's Far-infrared 220 cm<sup>-1</sup> Cloud. *Astrophys. J. Lett.* **761**, L15 (2012).
- Vinatier, S. et al. Seasonal variations in Titan's middle atmosphere during the northern spring derived from Cassini/CIRS observations. *Icarus* **250**, 95–115 (2015).
- Teanby, N. A. et al. Seasonal evolution of Titan's stratosphere during the Cassini mission. *Geophys. Res. Lett.* **46**, 3079–3089 (2019).
- Vinatier, S. et al. Study of Titan's fall southern stratospheric polar cloud composition with Cassini/CIRS: detection of benzene ice. *Icarus* **310**, 89–104 (2018).
- de Batz de Trenquelléon, B. et al. The new Titan planetary climate model. I. Seasonal variations of the thermal structure and circulation in the stratosphere. *Planet. Sci. J.* **6**, 78 (2025).
- de Batz de Trenquelléon, B., Rannou, P., Burgalat, J., Lebonnois, S. & d'Ollone, J. V. The new Titan planetary climate model. II. Titan's haze and cloud cycles. *Planet. Sci. J.* **6**, 79 (2025).
- Hanson, L. E., Waugh, D., Barth, E. & Anderson, C. M. Investigation of Titan's south polar HCN cloud during southern fall using micro-physical modeling. *Planet. Sci. J.* **4**, 237 (2023).
- Rannou, P., Le Mouélic, S., Sotin, C. & Brown, R. H. Cloud and haze in the winter polar region of Titan observed with Visual and Infrared Mapping Spectrometer on board Cassini. *Astrophys. J.* **748**, 4 (2012).
- Vinatier, S. et al. Temperature and chemical species distributions in the middle atmosphere observed during Titan's late northern spring to early summer. *Astron. Astrophys.* **641**, A116 (2020).
- Sharkey, J. et al. Potential vorticity structure of Titan's polar vortices from Cassini CIRS observations. *Icarus* **354**, 114030 (2021).
- Schinder, P. J. et al. The structure of Titan's atmosphere from Cassini radio occultations: occultations from the prime and equinox missions. *Icarus* **221**, 2 (2012).
- Mitchell, J. L., Ádámkóvics, M., Caballero, R. & Turtle, E. P. Locally enhanced precipitation organized by planetary-scale waves on Titan. *Nat. Geosci.* **4**, 9 (2011).
- Burgalat, J. & Rannou, P. Brownian coagulation of a bi-modal distribution of both spherical and fractal aerosols. *J. Aer. Sci.* **105**, 151–165 (2017).
- Burgalat, J., Rannou, P., Cours, T. & Rivière, E. D. Modeling cloud microphysics using a two-moments hybrid bulk/bin scheme for use in Titan's climate models: application to the annual and diurnal cycles. *Icarus* **231**, 310–322 (2014).
- Anderson, C. M., Samuelson, R. E. & Nna-Mvondo, D. Organic Ices in Titan's Stratosphere. *Space Sci. Rev.* **214**, 8 (2018).
- Dubois, D. et al. Investigating the condensation of benzene (C<sub>6</sub>H<sub>6</sub>) in Titan's south polar cloud system with a combination of laboratory, observational, and modeling tools. *Planet. Sci. J.* **2**, 4 (2021).
- de Batz de Trenquelléon, B., Rannou, P., Lebonnois, S. & Vinatier, S. *Genesis, Life, and Death of the Titan's Polar Clouds [Dataset]*. <https://doi.org/10.14768/85b9e037-57a2-46b5-945b-23a02e32aca2> (IPSL, 2025).

## Acknowledgements

We acknowledge support from the Grand Équipement National de Calcul Intensif (GENCI, allocation A0120110391) and from ROMEO (Université de Reims Champagne-Ardenne), where the Titan PCM simulations were performed.

## Author contributions

B.B.T. conceived the research, performed the calculations and wrote the manuscript. P.R. contributed to manuscript writing. P.R., S.L., and S.V. assisted with analysis.

## Competing interests

The authors declare no competing interests.

## Additional information

**Supplementary information** The online version contains supplementary material available at <https://doi.org/10.1038/s41467-025-66955-7>.

**Correspondence** and requests for materials should be addressed to Bruno de Batz de Trenquelléon.

**Peer review information** *Nature Communications* thanks Lavender Hanson, and the other anonymous, reviewer(s) for their contribution to the peer review of this work. A peer review file is available.

**Reprints and permissions information** is available at <http://www.nature.com/reprints>

**Publisher's note** Springer Nature remains neutral with regard to jurisdictional claims in published maps and institutional affiliations.

**Open Access** This article is licensed under a Creative Commons Attribution-NonCommercial-NoDerivatives 4.0 International License, which permits any non-commercial use, sharing, distribution and reproduction in any medium or format, as long as you give appropriate credit to the original author(s) and the source, provide a link to the Creative Commons licence, and indicate if you modified the licensed material. You do not have permission under this licence to share adapted material derived from this article or parts of it. The images or other third party material in this article are included in the article's Creative Commons licence, unless indicated otherwise in a credit line to the material. If material is not included in the article's Creative Commons licence and your intended use is not permitted by statutory regulation or exceeds the permitted use, you will need to obtain permission directly from the copyright holder. To view a copy of this licence, visit <http://creativecommons.org/licenses/by-nc-nd/4.0/>.

© The Author(s) 2025